台灣夏季降雨率估計

楊　傳　琮

氣象衛星中心

摘要

使用 Limin Zhao 的陸地上降雨率反演原理，由 AMSUA 第 1 及第 2 頻道 AMSUB 的 5 個頻道去估計降雨率，無雨區的準確率約爲 92%，有雨區的準確率約爲 83%，整體平均準確率爲 87%，降雨率偏差值的平均爲 3.6mm/hr。

一、前言

台灣位於西太平洋西側及亞洲大陸之東南隅，六月至九月受到梅雨、西南季風及颱風季降水的影響，是台灣主要的雨季。當有豪大雨發生時，往往伴隨著洪水氾濫、坍方、土石流、堤防潰決等災害，造成國家人民金錢財產的損失，對於最近雨年發生的納莉颱風及嘉義八掌溪事件，大家應該都還記憶猶新，能夠了解天然災害的可怕。由於人類對於大自然的過度開發或是開發不當，已經產生氣候反常，在極短的時間內就能降下極大的降雨量，人們對於以往熟悉的天氣型態也漸漸的感覺到有些生疏；氣象單位或是氣象學家對於天氣現象的掌握也愈是不易，因此須要一些較新式的氣象觀測儀器以提升氣象觀測及天氣預報的品質。隨著時代的進步，氣象觀測儀器也日新月異，如氣象雷達方面有都卜勒雷達、NEXRAD 等；氣象衛星方面有同步衛星，如 GMS、GOES 等；有繞極軌道衛星，如 NOAA、DMSP、EOS 資源衛星、TRMM 等等，其目的都是要增進氣象觀測的準確度以及時間、空間解析度的提升，以能增進氣象預報的準確度。參考張惠玲、　林沛練(1988)可知當要分析夏季午後對流降水時，如果只用傳統探空資料，每日只有 00Z 和 12Z 兩次觀測，在時間上是不夠多的；而探空站的分布方面則有板橋、花蓮、馬公、東港、綠島等站，在空間上亦顯得不足，如欲解析較小尺度的天氣現象，必須有高時間、高空間的解析度的觀測資料。

二、資料及研究方法

資料的來源主要爲本局的氣象資料，如 NOAA16，NOAA17衛星的資料，本局雷達回波圖及氣候資料庫自動雨量站的資料，以及颱風資料庫颱風路徑圖。參考(Weng and Grody 2000)，導出之公式

$$T_B(Zt,\mu)=\frac{T_B(Z_b,\mu)}{1+\Omega(\mu)} \quad \text{.....(1)}$$

Z_t和Zb分別爲雲頂和雲底的高度，μ是天頂角的餘弦亦即μ=cosθ，θ 爲天頂角，$T_B(Zt,\mu)$爲天頂角爲 θ 時由冰雲所放射出之亮度溫度，亦即由衛星所觀測之亮度溫度；$T_B(Zb,\mu)$爲天頂角爲 θ 時於雲底所觀測之亮度溫度，可由晴空區導出之經驗公式去計算。　則IWP(ice water path)可表示爲

$$IWP=\mu De\rho i(\Omega/\Omega_N) \quad \text{.....(2)}$$

ρi 爲冰水粒子的體密度(bulk volume density)，Ω_N是標準化的散射參數，De則是粒子有效半徑，降雨率 rr 則可表示爲

$$rr=C_0+C_1IWP+C_2IWP^2 \quad \text{.....(3)}$$

估算出降雨率後和3km內之自動雨量站比對，並且和雷達回波比對其類型，C_0, C_1, C_2 是由NOAA的網站得到的係數。

三、結果與討論

1. Limin Zhao 反演原理估算出降雨率，和3km內之自動雨量站比對，其結果列於表1 ，其統計結果列於表2，可知無雨的準確率約爲92%，有雨的準確率約爲83%，平均準確率爲87%，而降雨率之偏差值的平均爲3.6mm/hr，整體而言當觀測站雨量較大時，反演值會低估，可能是將AMSUA第一及第二頻道代入廻歸式，當降雨量較大時，亮度溫度因爲受到較大雨滴及冰粒子的散射作用而降低很多，因此在計算雲底亮度溫度時受到影響 。

2. 2004年6月28日至2004年7月4日有一個敏督利颱風侵襲台灣，造成嚴重的災害，它的路徑圖顯示於圖1，我們反演出2004年7月1日1749Z NOAA16降雨率圖且找出1800Z雷達回波圖與之比對，分別顯示於圖3圖2，1800Z自動雨量站降雨率則顯示於圖4，我們發現降雨率圖和雷達回波圖類型(pattern)相似，但是反演值較自動雨量站爲低。

四、結論

1.Limin Zhao的反演原理對於冰雲或是較大散射指數較敏感，因此反演數目較少，但是可以找到降雨率較大的地區。

2.反演降雨率值較自動雨量站降雨率值爲低，或許調整一些係數可以得到較好的結果。

五、參考文獻

張惠玲、林沛練，1998：台灣地區午後對流降水之研究，天氣分析與預報研討會論文彙編(87)，78-83。

Weng, F., and N.C.Grody, 2000：Retrieval of ice cloud parameters using a microwave imaging radiometer. J. Atmos. Sci., 57，1069-1081.

Zhao, L. and Weng, F.，2002：Retrieval of ice cloud parameters using the advanced microwa sounding unit. J. Apple. Meteor., 41，384-395.

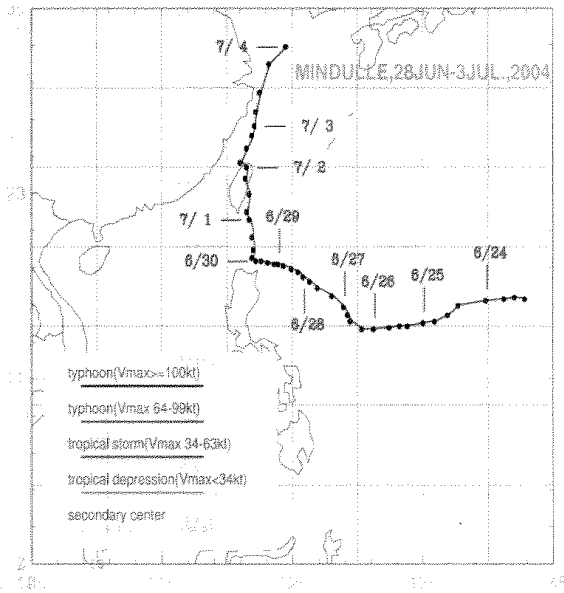

圖 1 敏 督 利 颱 風 路 徑 圖

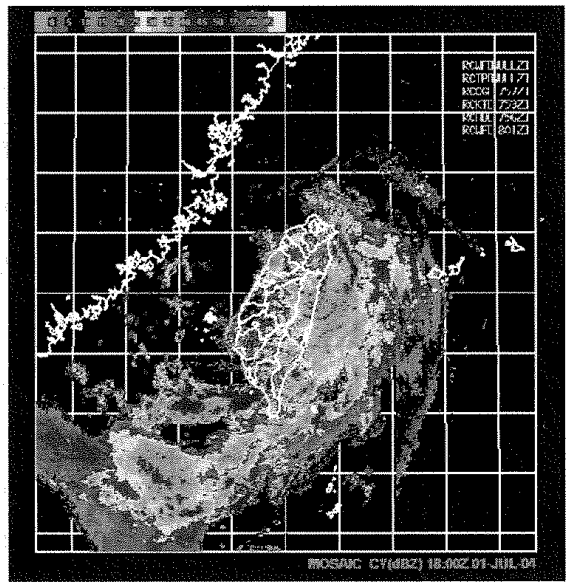

圖2 2004年7月1日1800Z雷達回波圖

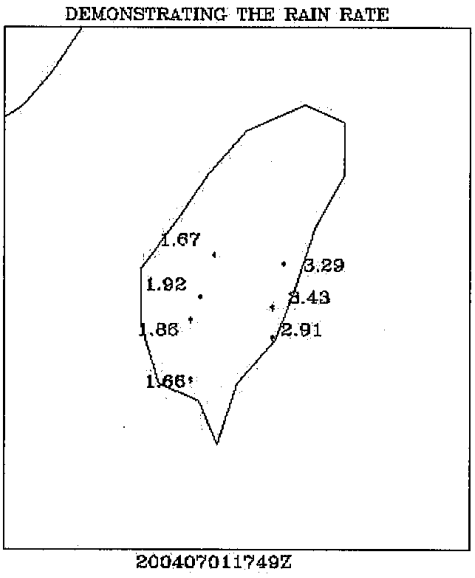

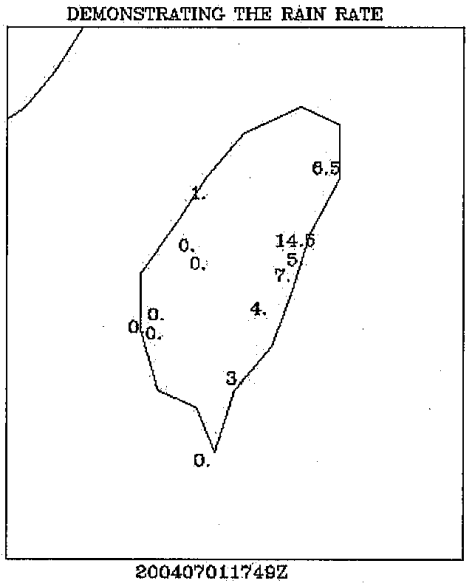

圖 3 2004年7月1日1749Z NOAA16降雨率圖　　圖4 2004年7月1日1800Z自動雨量站降雨率

項次	自動雨量	時間	自動雨量站雨量	反演雨量值	差值
1	福山	020710446	2.0	4.12	-2.1
2	美濃	0207170509	11.5	1.09	10.4
3	民生	0207170509	9.0	2.2	6.8
4	翠巒	0207170509	18.0	3.3	14.7
5	公館	0207170509	2.5	0.39	2.1
6	桃園	0207170509	0.0	0.0	0.0
7	民生	0207180458	11.0	0.47	10.5
8	上谷關	0207180458	3.0	0.44	2.56
9	摩天	0208020534	0.0	0.0	0.0
10	山豬湖	0307090554	0.0	1.95	-1.95
11	觀霧	0307090554	0.0	0.0	0.0
12	觀霧	0307230229	0.0	0.0	0.0
13	公館	0307230229	0.0	0.0	0.0
14	鼻頭角	0308130255	0.0	0.77	-0.77
15	大豹	0308130602	2.5	1.1	1.4
16	大豹	0308140232	0.0	0.0	0.0
17	翠巒	0308140232	0.0	0.0	0.0
18	南庄	0308140232	0.0	0.0	0.0

19	善化	0308140232	0.0	0.0	0.0
20	大棟山	0308140551	0.0	0.0	0.0
21	土庫	0308140551	0.0	0.0	0.0
22	觀霧	0308140551	0.0	0.0	0.0
23	四十份	0308140551	0.0	0.0	0.0
24	瑞芳	0308150211	0.0	0.0	0.0
25	石牌	0308150211	0.0	0.0	0.0
26	士林	0308150211	0.0	0.0	0.0
27	大棟山	0308150211	0.0	0.0	0.0
28	古亭坑	0308150211	0.0	0.0	0.0
29	觀霧	0308150540	0.0	0.0	0.0
30	永和	0308150540	0.0	0.0	0.0
31	西林	0308190219	0.5	0.0	0.5
32	東壙	0308190219	0.0	0.0	0.0
33	南州	0308240539	0.0	0.0	0.0
34	古亭坑	0308240539	0.0	0.0	0.0
35	斗六	0308240539	4.0	3.3	0.7
36	翠巒	0308240539	0.5	1.5	-1.0
37	觀霧	0308240539	6.5	0.0	6.5

表1陸地上反演之降雨率值和自動雨量站比較

	Accuracy of diagnose	Rms of rain rate	Sample size
Rain		3.6mm/nr	12
No-rain	92%		25
Total or mean	87%		37

表 2 陸地上反演之降雨率值和自動雨量站比較統計結果

model. The domain for the nonlinear and adjoint model is a 60-km, 85 x 115 (latitude by longitude) horizontal grid, with 20 sigma levels in the vertical. The initial and boundary conditions are from the NCEP GFS (Global Forecasting System) global analysis (1 ° x 1 °) interpolated to the MM5 grids.

Typhoon Mindulle in 2004, one that was observed in DOTSTAR, is chosen as a test case to examine the proposed new method for targeted observations based on the adjoint sensitivity. Note that Mindulle is the sole case out of the ten DOTSTAR cases in 2004 where dropsonde data assimilated into the NCEP GFS model did not improve the track forecasts (figures not shown). The study is based on a 36-h MM5 simulation initialized at 1200 UTC 27 June 2004. The 'forward' and 'backward' integrations were executed by the MM5 forecast model and the adjoint model, respectively, as indicated in Fig. 1. The 'negative' sign in front of the time indicates the 'backward' integration (using the negative timestep) associated with the adjoint model. Figure 2 shows that the model storm moves along (but slightly faster than) the best track from the Central Weather Bureau (CWB) of Taiwan.

The work is aimed to identify the sensitive areas at the observing time (1200 UTC 27 June), which will affect the steering flow of Typhoon Mindulle at the verifying time (0000 UTC 29 June). Therefore, we define the response function(s) as the deep-layer mean wind within the verifying area. A square of 600 km by 600 km, centered around the MM5-simulated storm location (Fig. 3) at the verifying time, is used to calculate the background steering flow (Chan and Gray 1982). Two responses functions are then defined: R_1, the 850-300-hPa deep-layer area average (Wu et al. 2003) of zonal component (u), and R_2, the average of meridional component (v) of the wind vector, i.e.,

$$R_1 \equiv \frac{\int_{850hPa}^{300hPa}\int_A u \quad dxdydp}{\int_{850hPa}^{300hPa}\int_A dxdydp}, \text{and}$$

$$R_2 \equiv \frac{\int_{850hPa}^{300hPa}\int_A v \quad dxdydp}{\int_{850hPa}^{300hPa}\int_A dxdydp}. \qquad (1)$$

In other words, by averaging out the axisymmetric component of the strong cyclonic flow around the storm center, the vector of (R_1, R_2) represents the background steering flow across the storm center at the verifying time (Note that this is a wind vector, which is totally different from the kinetic energy norm described above).

In order to interpret the sensitivity with clear physical meanings, we design a unique new parameter, Adjoint-Derived Sensitivity Steering Vector (ADSSV), to identify the sensitive areas at the observing time to the steering flow at the verifying time. The ADSSV with respect to the vorticity field (ς) can be shown as

$$ADSSV \equiv \left(\frac{\partial R_1}{\partial \varsigma}, \frac{\partial R_2}{\partial \varsigma}\right), \qquad (2)$$

Where, at a given point, the magnitude of ADSSV indicates the extent of the sensitivity, and the direction of the ADSSV represents the change in the response of the steering flow with respect to a vorticity perturbation placed at that point. For example, if at a given forecast time at at one particular grid point the ADSSV vector points to the east, an increase of the vorticity at that same point at the observing time would be associated with an increase of the eastward steering of the storm at the verifying time.

3. Results

Based on Eq. (1), we first show that the background steering flow (R_1, R_2) at the verifying time in MM5 is (-6.7 m s-1, -0.8 m s-1), which is consistent with the model's westward movement of Mindulle at the verifying time (see the model's storm track in Fig. 2). In this paper, only the sensitivity products at 700 hPa are shown. In general, the results of the sensitivity patterns either at 850 or at 500 hPa are qualitatively consistent with one another.

As expected, the sensitivity (i.e., gradient) of R_1 to u (R_1/ u) at 0 h (the initial time of adjoint model) shows a response uniformly distributed over the verifying area (Fig. 3a), while there is no sensitivity of R_1 to v (R_1/ v) (Fig. 3b). To show a general sensitivity to the wind field, we combine the sensitivity of R_1 to u and the sensitivity of R_1 to v to obtain the sensitivity of R_1 to the vorticity field [$\partial R_1/\partial \varsigma$] (see the derivation in Kleist and Morgan 2005). Again, as expected, a dipolar pattern at 0 h (Fig. 3c) is found, i.e., a positive (negative) vorticity perturbation to the north (south) of the verifying area is associated with a cyclonic (anticyclonic) circulation and thus leads to an increase in R_1 (the zonal component of the mean steering flow). Meanwhile, the sensitivity of R_2 to u, v, and the vorticity field (Figs. 3d, e, and f) also reveals comparable information. In all, Figs. 3c and 3f can succinctly show the sensitivity of R_1 and R_2 to the flow field with clear physical meanings.

The evolutions of the sensitivity of R_1 and R_2 to the vorticity field are shown in Figs. 4 and 5. The sensitive areas spread from the margin of the verifying area to the outer region as the adjoint model is integrated backward in time. At –36 h (the observing time, 1200 UTC 27 June), the large gradient (and thus the high sensitivity) areas are located in the east and north of the verifying area, and the sensitivity is found to be higher in R_2 than in R_1. This means that vorticity perturbations in those large gradient (sensitive) areas at 1200 UTC 27 June will affect the steering flow of Typhoon Mindulle at 0000 UTC 29 June, particularly the meridional component of the steering flow.

As shown in Eq. (2), we can combine the result of Figs. 4 and 5 to obtain the evolution of ADSSV with respect to the vorticity field (Fig. 6). Figure 6 clearly shows that the vectors rotate around the verifying area at 0 h. As the adjoint model integrates backward in time, these vectors evolve and expand outward, with longer

氣候監測與預測

Climate Monitoring and Prediction

氣候監測與預測

Climate Monitoring and Prediction